Spin filter for arbitrary spins by substrate engineering

Biplab Pal,[1,*] Rudolf A. Römer,[2,†] and Arunava Chakrabarti[1,‡]

[1] *Department of Physics, University of Kalyani, Kalyani, West Bengal-741235, India*
[2] *Department of Physics and Centre for Scientific Computing, University of Warwick, Coventry, CV4 7AL, UK*

We design spin filters for particles with potentially arbitrary spin S (= 1/2, 1, 3/2, ...) using a one-dimensional periodic chain of magnetic atoms as a quantum device. Describing the system within a tight-binding formalism we present an analytical method to unravel the analogy between a one-dimensional magnetic chain and a multi-strand ladder network. This analogy is crucial, and is subsequently exploited to engineer gaps in the energy spectrum by an appropriate choice of the magnetic substrate. We obtain an exact correlation between the magnitude of the spin of the incoming beam of particles and the magnetic moment of the substrate atoms in the chain desired for opening up of a spectral gap. Results of spin polarized transport, calculated within a transfer matrix formalism, are presented for particles having half-integer as well as higher spin states. We find that the chain can be made to act as a quantum device which opens a transmission window only for selected spin components over certain ranges of the Fermi energy, blocking them in the remaining part of the spectrum. The results appear to be robust even when the choice of the substrate atoms deviates substantially from the ideal situation, as verified by extending the ideas to the case of a 'spin spiral'. Interestingly, the spin spiral geometry, apart from exhibiting the filtering effect, is also seen to act as a device flipping spins – an effect that can be monitored by an interplay of the system size and the period of the spiral. Our scheme is applicable to ultracold quantum gases, and might inspire future experiments in this direction.

PACS numbers: 72.25.Mk, 85.75.-d

I. INTRODUCTION

The idea of transporting information through electron spins instead of charge, *spintronics* [1, 2], has opened a promising pathway to quantum information processing and quantum computation in the future. Spurred by the measurement of tunneling magnetoresistance in magnetic tunnel junctions [3, 4], and the observation of giant magneto-resistance in magnetic multilayers [5], the search for the integration of memory and logic in a single storage device has taken an inspiring shape in the last couple of decades.

A substantial part of the existing research focuses on experiments related to spin polarized electron transport in nanostructures. The quantum confinement effect on transport of electrons was studied by several groups [6–8]. Tunable spin filters have been developed where charge carriers with different spin states were separated in GaAs samples [9]. A 'non-local' spin valve geometry was used to study spin transport in single graphene layers [10]. Experimental realizations of a quantum spin pump using a GaAs quantum dot [11], an 'open' quantum dot driven by ac gate voltages [12], along with several other works such as the study of spontaneous spin polarized transport in magnetic nanowires [13] or, an analysis of the spin polarization of the linear conductance of a quantum wire spin filter [14], have enriched the field of spin polarized transport. The design of molecular wires and spin polarized tunneling devices [15] is also in the cards in the current era of spintronics.

Needless to say, such experiments have inspired a bulk of theoretical investigations of spin transport, or spin polarized coherent electronic transport in nano structures, in model quantum dots or magnetic nanowires [16–24], or, in a very recent work, modeling a ferroelectric polymer grown on top of a silicene nanoribbon [25]. A widely adopted line of attack has been to work within a tight-binding formalism in which a nano wire is simulated by placing 'magnetic atoms' in a line, and sandwiching the array between two semi-infinite magnetic or non-magnetic leads [19–24]. Green's function method and transfer matrix techniques [29, 30] are then used to extract spectral information and linear conductance. Though simple enough, such model studies indeed bring out some subtleties of coherent spin dependent electronic transport, often showing the spin filtering effect over selected ranges of energy [24].

Some recent studies on spin-based transistor [26–28] reveal the fact that spin transmission can be controlled by a suitable combination of a homogeneous magnetic field and a helical magnetic field in two-dimensional magnetic semiconductor waveguide structures. The relative strength of the homogeneous and helical field components controls the backscattering process of the spins which changes conductance and the degree of spin polarization of transmitted electrons, and the device can be switched into 'off' or 'on' state. In contrast to this, in the present study we try to explore the role of the local magnetic moments of the magnetic atomic sites in the chain to control

*Electronic address: biplabpal@klyuniv.ac.in
†Electronic address: r.roemer@warwick.ac.uk
‡Electronic address: arunava_chakrabarti@yahoo.co.in

the spin transmission for particles with spin 1/2 as well as higher spin states in such model magnetic quantum device.

While spin polarized transport of electrons has been the main concern so far, transport of particles with spins higher than that of an electron, even in one dimension (1D), has not received the same level of attention. This is, to our mind, an area which needs to be explored in order to unravel the possibility of designing novel storage devices which rely on the transportation or spin filtering of ultracold bosonic or fermionic quantum gases exhibiting higher spin states. Spin-3/2 particles, for example, can be realized with alkali atoms of ^{6}Li, ^{132}Cs, and alkaline earth atoms of ^{9}Be, ^{135}Ba, and ^{137}Ba. These large-spin atomic fermions display diverse many-body phenomena, and can be realized experimentally through controlled interactions in spin scattering channels [31]. Experimentally realized 1D strongly correlated liquids of ultracold fermions with a tunable number of spin components [32], spin polarized hydrogen which remains gaseous down to zero temperature, and happens to be a good candidate for realizing Bose condensation in a dilute atomic gas, or a gas of ultracold ^{52}Cr atoms forming a dipolar gas of high spin atoms [33], are some of the recently developed quantum systems which provide a versatile and robust platform for probing fundamental problems in condensed matter physics, as well as finding applications in quantum optics and quantum information processing.

Thus the availability of high spin state particles opens up an unexplored area of engineering spin filters for spins higher than $S = 1/2$. It is already appreciated that [31], in contrast to the conventional spin-1/2 electronic case, large-spin ultracold atomic fermions, even in 1D, exhibit richer spin phenomena. Thus, exploring the possibility of selecting out a state with a definite spin projection using a suitable quantum device might lead to innovative manipulation and control of spin transport. This precisely, is the motivation of the present communication.

We get exciting results. Using a simple 1D chain of magnetic atoms, mimicking a quantum gas in an artificial periodic potential, we show within a tight-binding framework that a suitable correlation between the spin S of the incoming beam of particles, and the magnetic moment $\vec{h}$ offered by the substrate atoms can open up a gap in the energy spectrum. The opening of the gap turns out to be crucial in transporting a given spin state over a specified range of Fermi energy, while blocking the remaining spin states. The simple 1D chain of magnetic atoms of spin S is shown to be equivalent to a $(2S+1)$-strand ladder network. This equivalence is exploited to work out the precise criterion of opening up of the spectral gap. The results seem to be robust against at least a minimal incorporation of disorder, as suggested by the results of spin polarized transport for a spin spiral, as reported in this communication.

In section II we describe the basic scheme in terms of the spin-1/2 and spin-1 particles. The difference equations are established which will finally be used to obtain the spectra in the respective cases. Section III describes how to engineer the spectral gaps using an appropriate substrate and provides the general criterion for opening up of the spectral gap for arbitrary spins. The discussion is substantiated by a detailed presentation of the density of states (DOS) choosing the spin-1/2 case as example. In section IV we present the results of the transport calculations for the spin-1/2 and spin-1 cases. In section V we discuss the idea of having a spin filtering with a correlated disorder. In section VI we show the robustness of the results by considering a spin-spiral where the substrate atoms have their magnetic moments turning sequentially, in a periodic fashion, mimicking disorder over a length shorter than the period, and in section VII we draw our conclusions. The appendices contain the details of the transport formulation, and further details are provided in the supplemental material.

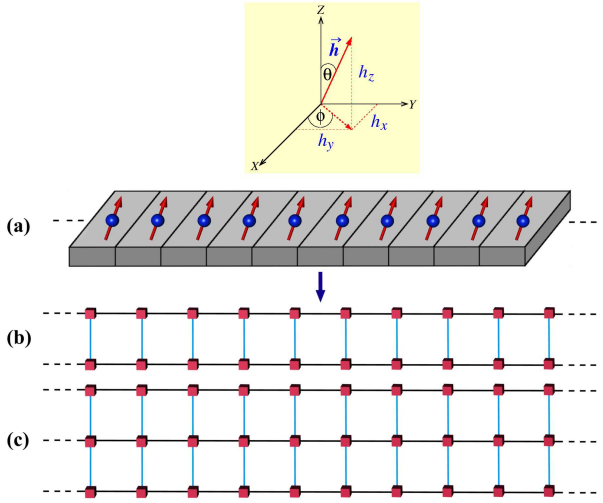

FIG. 1: (Color online) (a) Schematic diagram of a linear magnetic chain grafted on a substrate (gray blocks). Each magnetic atom (blue sphere) is subject to a substrate-induced magnetic moment $\vec{h} = (h_x, h_y, h_z)$ (red arrow) making an angle θ with the z axis and ϕ is the azimuthal angle. (b) Schematic representation of a two-strand ladder network with solid lines denoting the hopping elements and cubes representing the effective "sites". (c) Schematic representation of a three-strand ladder network. The decomposition of $\vec{h}$ into its components is shown in the inset box above the magnetic chain.

II. MODELLING A SPIN S CHAIN AS A LADDER OF WIDTH $2S+1$

In Fig. 1 we propose a model system consisting of a linear array of *magnetic* atoms grafted on a substrate. The atom at the n-th site has a magnetic moment $\vec{h}_n$ associated with it. The Hamiltonian in the tight-binding

approximation can be written as

$$\boldsymbol{H} = \sum_n \boldsymbol{c}_n^\dagger \left(\boldsymbol{\epsilon}_n - \vec{h}_n \cdot \boldsymbol{S}_n^{(S)}\right) \boldsymbol{c}_n + \sum_{\langle n,m\rangle} \boldsymbol{c}_n^\dagger \boldsymbol{t}_{n,m} \boldsymbol{c}_m + \boldsymbol{c}_m^\dagger \boldsymbol{t}_{n,m} \boldsymbol{c}_n, \quad (1)$$

with $\langle n, m\rangle$ denoting nearest neighbors, *i.e.*, $m = n \pm 1$. Each of the quantities $\boldsymbol{c}_n^\dagger$, $\boldsymbol{c}_n$, $\boldsymbol{\epsilon}_n$, $\boldsymbol{t}_{n,m}$ and $\boldsymbol{S}_n^{(S)}$ denotes a multi-component expression according to the spin content, *i.e.*, for the $S = 1/2$ case, $\boldsymbol{c}_n^\dagger = (c_{n,\uparrow}^\dagger, c_{n,\downarrow}^\dagger)$ is the creation operator at the nth site, $\boldsymbol{\epsilon}_n = \mathrm{diag}\,(\epsilon_{n,\uparrow}, \epsilon_{n,\downarrow})$ describes the diagonal on-site potential matrix, and $\boldsymbol{t}_{n,m} = \boldsymbol{t} = \mathrm{diag}\,(t, t)$ encodes the uniform nearest-neighbor hopping integral t along n. The indices '↑', '↓' refer to the spin projections (spin 'channels') for the case $S = 1/2$.

It is easily appreciated that the dimensions of the matrices increase proportionately as one extends the scheme to spin 1, 3/2 or higher values. Consequently, the creation and the annihilation operators will also have multiple components indexed by every single value of the spin projection $m_S = -S, -S+1, \ldots, S-1, S$, having a total of $2S + 1$ values for a general spin-S particle. The term $\vec{h}_n \cdot \boldsymbol{S}_n^{(S)} = h_{n,x}\boldsymbol{S}_{n,x}^{(S)} + h_{n,y}\boldsymbol{S}_{n,y}^{(S)} + h_{n,z}\boldsymbol{S}_{n,z}^{(S)}$ describes the interaction of the spin (S) of the injected particle with the localized on-site magnetic moment $\vec{h}_n$ at site n. This term is responsible for spin flipping at the magnetic sites. For $S = 1/2, 1, 3/2, \ldots$, the $\boldsymbol{S}_x$, $\boldsymbol{S}_y$, $\boldsymbol{S}_z$ denote the generalized Pauli spin matrices $\boldsymbol{\sigma}_x$, $\boldsymbol{\sigma}_y$, $\boldsymbol{\sigma}_z$ expressed in units of $\hbar S$. Spin flip scattering is hence dependent on the orientation of the magnetic moments $\vec{h}_n$ in the magnetic chain with respect to the z axis. Written explicitly for $S = 1/2$ we have

$$\vec{h}_n \cdot \boldsymbol{S}_n^{(1/2)} = h_{n,x}\boldsymbol{\sigma}_x + h_{n,y}\boldsymbol{\sigma}_y + h_{n,z}\boldsymbol{\sigma}_z = \begin{pmatrix} h_n\cos\theta_n & h_n\sin\theta_n e^{-i\phi_n} \\ h_n\sin\theta_n e^{i\phi_n} & -h_n\cos\theta_n \end{pmatrix}, \quad (2)$$

with θ_n and ϕ_n denoting polar and azimuthal angles, respectively.

The time-independent Schrödinger equation for the pure spin-1/2 system is written as $H|\chi\rangle = E|\chi\rangle$, where $|\chi\rangle = \sum_n \left(\psi_{n,\uparrow}|n,\uparrow\rangle + \psi_{n,\downarrow}|n,\downarrow\rangle\right)$ is a linear combination of spin-*up* (↑) and spin-*down* (↓) Wannier orbitals. Operating H on $|\chi\rangle$ we get two equations relating the $\psi_{n,\uparrow}$, $\psi_{n,\downarrow}$ amplitudes on position n with the neighboring $n \pm 1$ sites,

$$(E - \epsilon_{n,\uparrow} + h_n\cos\theta_n)\,\psi_{n,\uparrow} + h_n\sin\theta_n e^{-i\phi_n}\psi_{n,\downarrow} = t\psi_{n+1,\uparrow} + t\psi_{n-1,\uparrow}, \quad (3a)$$

$$(E - \epsilon_{n,\downarrow} - h_n\cos\theta_n)\,\psi_{n,\downarrow} + h_n\sin\theta_n e^{i\phi_n}\psi_{n,\uparrow} = t\psi_{n+1,\downarrow} + t\psi_{n-1,\downarrow}. \quad (3b)$$

Eqs. (3a) and (3b) can be expressed in compact form as matrix equation of the form,

$$(E\mathbf{1} - \tilde{\boldsymbol{\epsilon}}_n)\boldsymbol{\psi}_n = \boldsymbol{t}\boldsymbol{\psi}_{n+1} + \boldsymbol{t}\boldsymbol{\psi}_{n-1}, \quad (4)$$

where

$$\tilde{\boldsymbol{\epsilon}}_n = \begin{pmatrix} \epsilon_{n,\uparrow} - h_n\cos\theta_n & -h_n\sin\theta_n e^{-i\phi_n} \\ -h_n\sin\theta_n e^{i\phi_n} & \epsilon_{n,\downarrow} + h_n\cos\theta_n \end{pmatrix}, \quad (5)$$

and $\boldsymbol{\psi}_n = (\psi_{n,\uparrow}, \psi_{n,\downarrow})$. We draw the attention of the reader to the equivalence of Eq. (3) to the difference equations for a *spinless* electron in a two-strand ladder network, as depicted in Fig. 1(b) with an effective on-site potential $\epsilon_{n,\uparrow} - h_n\cos\theta_n$, and $\epsilon_{n,\downarrow} + h_n\cos\theta_n$ for the 'upper' strand (identified with ↑ component) and the 'lower' strand (identified with ↓ component) respectively. The amplitude of the hopping integral along each arm of the ladder is t, while $h_n\sin\theta_n\exp(i\phi_n)$ plays the role of *inter-strand* hopping integral along the n-th strand [34].

Similarly, for spin $S = 1$ particles, we have $2S + 1 = 3$ coupled equations analogous to Eq. (3), namely,

$$[E - (\epsilon_{n,1} - h_n\cos\theta_n)]\,\psi_{n,1} + \frac{1}{\sqrt{2}}h_n\sin\theta_n e^{-i\phi_n}\psi_{n,0} = t\psi_{n+1,1} + t\psi_{n-1,1}, \quad (6a)$$

$$[E - \epsilon_{n,0}]\,\psi_{n,0} + \frac{1}{\sqrt{2}}h_n\sin\theta_n e^{i\phi_n}\psi_{n,1} + \frac{1}{\sqrt{2}}h_n\sin\theta_n e^{-i\phi_n}\psi_{n,-1} = t\psi_{n+1,0} + t\psi_{n-1,0}, \quad (6b)$$

$$[E - (\epsilon_{n,-1} + h_n\cos\theta_n)]\,\psi_{n,-1} + \frac{1}{\sqrt{2}}h_n\sin\theta_n e^{i\phi_n}\psi_{n,0} = t\psi_{n+1,-1} + t\psi_{n-1,-1}. \quad (6c)$$

for the three spin projections, viz., +1, 0 and −1. The 3×3 matrix for the 'effective' on-site potential at the n-th position now reads,

$$\tilde{\boldsymbol{\epsilon}}_n = \begin{pmatrix} \epsilon_{n,1} - \lambda_n & -\frac{1}{\sqrt{2}}\xi_n e^{-i\phi_n} & 0 \\ -\frac{1}{\sqrt{2}}\xi_n e^{i\phi_n} & \epsilon_{n,0} & -\frac{1}{\sqrt{2}}\xi_n e^{-i\phi_n} \\ 0 & -\frac{1}{\sqrt{2}}\xi_n e^{i\phi_n} & \epsilon_{n,-1} + \lambda_n \end{pmatrix}, \quad (7)$$

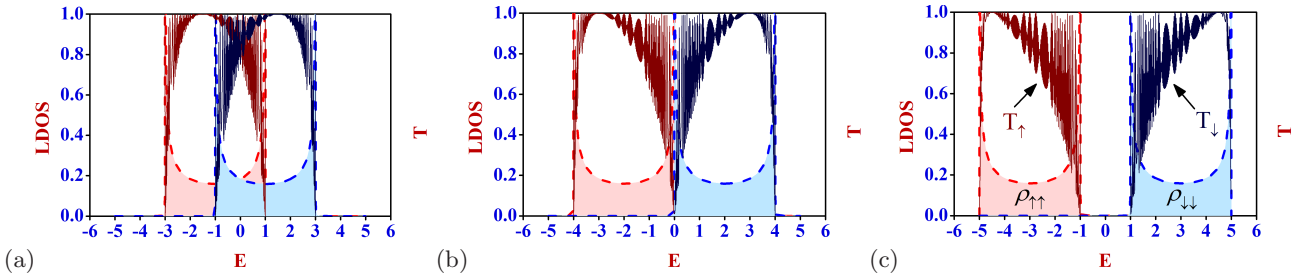

FIG. 2: (Color online) Variation of local density of states (LDOS) and transmission probabilities with energy E as a function of h for a fixed value of $\theta = 0$ for spin-1/2 particles. The light red shaded plot with red envelope is the LDOS for the spin-up ($\uparrow$) states and the light blue shaded plot with blue envelope is the LDOS for the spin-down ($\downarrow$) states. The dark red curve represents the transmission characteristics for the spin-up ($\uparrow$) particles and the dark blue curve is exhibiting the transport for the spin-down ($\downarrow$) particles. (a) is for $h = 1$, (b) is for $h = 2$, and (c) corresponds to $h = 3$. The lead parameters for the non-magnetic leads are $\epsilon_L = \epsilon_R = 0$ and $t_{LD} = t_{RD} = t_L = t_R = 3$.

where $\lambda_n = h_n \cos\theta_n$ and $\xi_n = h_n \sin\theta_n$. Clearly, this can be extended to treat the case of general S, leading to an effective ladder model with $2S + 1$ arms as shown in Fig. 1. The above equations, viz., Eq. (3) and Eq. (6) will now be exploited to engineer the spectral gaps and simulate spin filters, as explained in the subsequent sections.

III. ENGINEERING THE SPECTRAL GAPS

1. *Computing the density of states*

Its instructive to remind ourselves as to when one can have a gap in the spectrum of such a ladder network in terms of the simplest possible case, where one can set $\epsilon_{n,\uparrow} = \epsilon_{n,\downarrow} = \epsilon_n = \epsilon$, a constant at all sites n of both the arms of the ladder, and $h_n = h$. We additionally set $\theta_n = \theta$ and $\phi_n = 0$. It is easy to understand that, in the extreme limit of $t \to 0$, the spectrum of the two-strand ladder yields sharply localized (pinned) eigenstates at $E = \epsilon \pm h$. The DOS will exhibit two δ-function spikes at these energy eigenvalues. As the hopping along the arms of the ladder, viz., t is switched 'on', the δ function like spikes in the DOS spectrum broaden into two subbands, which will finally merge into a single band when $h \sim t$. Therefore, for a given value of the polar angle θ, and a predefined value of t (which sets the scale of energy), the inter-strand hopping h can be tuned to open or close a gap in the energy spectrum.

Mapping back onto the original 1D magnetic chain the above argument clearly shows that one can create gaps in the spectrum or close them, by a judicious engineering of the substrate, that is, the required species of the magnetic atoms providing an appropriate value of the magnetic moment h. This simple argument allows us to gain analytical control over the spectrum and eventually turns out to be crucial in designing a spin filter. In Fig. 2 we show the DOS of a uniform magnetic chain with $\theta = 0$, and $\phi = 0$. The DOS for the 'up' and the 'down' spin electrons in the magnetic chain with $\epsilon = 0$ and $t = 1$ have been calculated by evaluating the matrix elements of the Green's function $\boldsymbol{G} = (E\mathbf{1} - \boldsymbol{H})^{-1}$ in the Wannier basis $|j, \uparrow (\downarrow)\rangle$. The local DOS (same as the average DOS in this case) for the 'up' and 'down' spin electrons are given by,

$$\rho_{\uparrow\uparrow(\downarrow\downarrow)} = \lim_{\eta \to 0} \langle j, \uparrow (\downarrow) | \boldsymbol{G}(E + i\eta) | j, \uparrow (\downarrow) \rangle. \tag{8}$$

Here, $\rho_{\uparrow\uparrow}$ and $\rho_{\downarrow\downarrow}$ have been evaluated using a real space decimation renormalization method elaborated elsewhere [38, 39].

2. *Substrate-induced opening and closing of spectral gaps*

The choice of the strength of the magnetic moment that will make the spectrum gapless is not quite arbitrary. One can, at least for a special relative orientation of the moments at the nearest neighboring sites, work out a prescription for this. To appreciate the scheme, let us observe that, even for a site dependent potential ϵ_n and the magnetic moment h_n, the commutator $[\tilde{\boldsymbol{\epsilon}}_n, \tilde{\boldsymbol{\epsilon}}_{n+1}] = 0$ if we choose $\theta_{n+1} - \theta_n = m\pi$, where $m = 0, \pm 1, \pm 2, \pm 3, ...$ and $\phi_n = \phi_{n+1} = 0$ or a constant value, irrespective of the values of ϵ_n or h_n. That is, the system may represent either a ferromagnetic alignment of the moments, or an antiferromagnetic one. Needless to say, the specific case of constant ϵ and constant θ falls in this category. In such cases, it is possible to decouple the matrix equation (4) into a set of two independent linear equations by making a change of basis, going from $\tilde{\boldsymbol{\psi}}_n$ to $\boldsymbol{\mathcal{F}}_n$, where, $\boldsymbol{\mathcal{F}}_n = \boldsymbol{S}^{-1}\tilde{\boldsymbol{\psi}}_n$. $\boldsymbol{S}$ executes a similarity transformation on Eq. (4). The commutation ensures that every $\tilde{\boldsymbol{\epsilon}}_n$ matrix can be diagonalized simultaneously by the same matrix $\boldsymbol{S}$. The concept has previously been used to study the electronic spectrum of disordered and quasiperiodic ladder networks [34–36], and 2D lattices with correlated disorder [37]. The decoupled equations read,

$$(E - \epsilon_n + h_n)\,\mathcal{F}_{n,\uparrow} = t\mathcal{F}_{n+1,\uparrow} + t\mathcal{F}_{n-1,\uparrow}, \tag{9a}$$
$$(E - \epsilon_n - h_n)\,\mathcal{F}_{n,\downarrow} = t\mathcal{F}_{n+1,\downarrow} + t\mathcal{F}_{n-1,\downarrow}, \tag{9b}$$

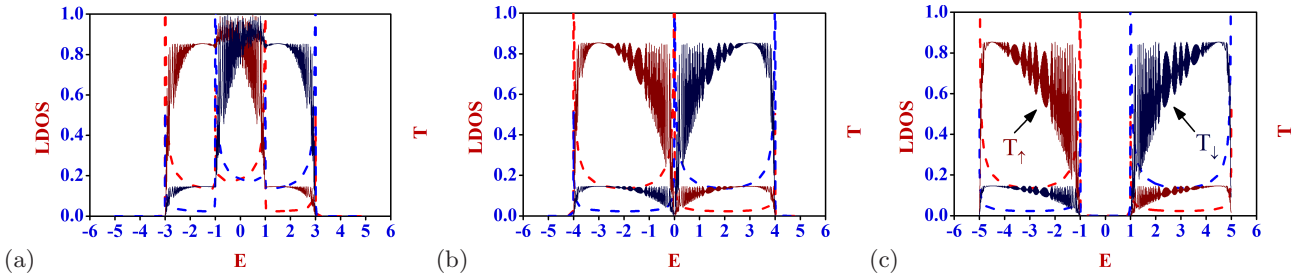

FIG. 3: (Color online) Variation of LDOS and transmission probabilities with energy E as a function of h for a fixed value of $\theta = \pi/4$ for spin-1/2 particles. The curves with the red dashed line represent the LDOS for the spin-up ($\uparrow$) states and the curves with the blue dashed line represent the LDOS for the spin-down ($\downarrow$) states. The dark red curve represents the transmission probability for the spin-up ($\uparrow$) particles and the dark blue curve is exhibiting the transmission probability for the spin-down ($\downarrow$) particles. (a) is for $h = 1$, (b) is for $h = 2$, and (c) corresponds to $h = 3$.

and represent the equations for two *pseudoparticles* with mixed spin states,

$$\mathcal{F}_{n,\uparrow} = \frac{\sin\theta_n}{2}\psi_{n,\uparrow} + \frac{1-\cos\theta_n}{2}\psi_{n,\downarrow}, \quad (10a)$$

$$\mathcal{F}_{n,\downarrow} = -\frac{\sin\theta_n}{2}\psi_{n,\uparrow} + \frac{1+\cos\theta_n}{2}\psi_{n,\downarrow}. \quad (10b)$$

The subscripts '$\uparrow$' or '$\downarrow$' in $\mathcal{F}_n$ can be taken to be the indices for the two decoupled arms of the equivalent two-strand ladder.

Let us again get back to the perfectly ordered case with $\epsilon_n = \epsilon$, and $h_n = h$. The first thing to appreciate is that each individual equation, viz., Eq. (9a) and Eq. (9b) now represents a perfectly periodic array of atomic like sites with an *effective* on-site potential $\epsilon \pm h$, and a constant nearest neighbor hopping integral t. Consequently they offer *absolutely continuous* energy bands, ranging from $\epsilon - h - 2t$ to $\epsilon - h + 2t$ corresponding to Eq. (9a), and $\epsilon + h - 2t$ to $\epsilon + h + 2t$ for the second decoupled equation Eq. (9b). The energy spectrum for the individual infinite chains can be obtained conventionally by working out the DOS for each of them. The DOS of the actual linear magnetic chain is then obtained through a convolution of these two individual DOS's. It is simple to compute that the gap between the bands is given by,

$$\Delta = 2h - 4t. \quad (11)$$

This immediately leads to a *critical* value of the strength of the magnetic moment $h_c = 2t$ for which the gap will *just* close. The result is independent of any arbitrary constant value of the polar angle θ, as long as one ensures that the difference between nearest neighboring values of the angle, viz., $\theta_{n+1} - \theta_n = m\pi$ ($m = 0, \pm1, \pm2, \pm3, ...$).

The variation of the DOS against energy as a function of h is a generic feature of the magnetic array for any constant value of the polar angle θ. This is evident from Figs. 2 and 3, where we have plotted the local density of states (LDOS) at a site in the infinite chain. For a periodic chain the LDOS is same as the average DOS. It is clear from the figures, how a gradual increase in the value of the magnetic moment h, a gap opens in the spectrum, going through a sequence of variations shown in each panel, where the values of $\rho_{\uparrow\uparrow}$ and $\rho_{\downarrow\downarrow}$ complement each other. To be noted that, in all the plots the energy E in the abscissa is taken in units of t.

3. *Spectral gaps for larger S*

A look at the set of Eq. (6) immediately reveals the equivalence of the magnetic chain in the present case with that of a three-strand ladder as depicted in Fig. 1(c). The effective on-site potential at the n-th vertex at every strand is given by $\epsilon_n - h_n\cos\theta_n$, ϵ_n and $\epsilon_n + h_n\cos\theta_n$ respectively, while the role of the inter-strand coupling (hopping integral) between the adjacent strands is played by $h_n\sin\theta_n/\sqrt{2}$ (with ϕ_n is set equal zero). As before, one can argue that an appropriate tuning of h_n (for a given value of $\theta_n = \theta$ = constant) should open up gaps in the spectrum, in the same way as it did in the spin-1/2 case. This is precisely what we see in Fig. 4. We have chosen a chain with a constant value of the on-site potential $\epsilon_n = \epsilon$, h_n has been fixed to any desired constant value, and $\theta_n = \phi_n = 0$. The left, middle and the bottom panels exhibit the overlap of bands for $h = 3$, the marginal case where the bands just touch each other for $h = 4$, and a clear opening of the gaps when $h = 6$, respectively. The location of the gaps can be estimated quite easily if one observes that with $\theta = 0$, the strands in the three-arm ladder effectively get decoupled, so that one is left with a set of three independent equations representing three individual ordered chains with on site potentials $\epsilon - h$, ϵ, and $\epsilon + h$ respectively. The corresponding ranges of eigenvalues are, $[\epsilon - h - 2t, \epsilon - h + 2t,]$, $[\epsilon - 2t, \epsilon + 2t]$, and $[\epsilon + h - 2t, \epsilon + h + 2t]$. The gap between these ranges can now be estimated in a straightforward way, and the critical value of h, for which gaps will open for any spin S can thus be worked out to be,

$$\Delta^{(S)} = \frac{h}{S} - 4t. \quad (12)$$

This equation holds for any spin, viz., $S = 1/2$, 1, 3/2, 2, 5/2, ... So in principle, we can engineer the bands

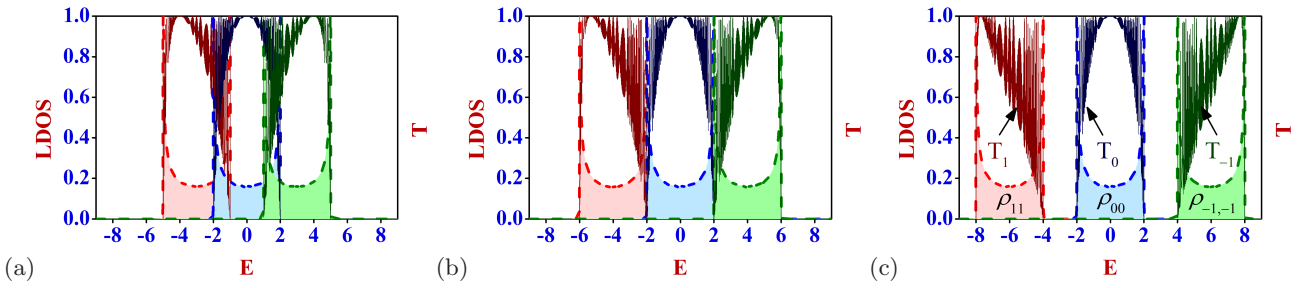

FIG. 4: (Color online) Variation of LDOS and transmission probabilities with energy E as a function of h for a fixed value of $\theta = 0$ for spin-1 particles. The light red shaded plot with the dashed red envelope is the LDOS for the spin-1 states, the light blue shaded plot with the blue dashed envelope is the LDOS for the spin-0 states, and the light green shaded plot with the green dashed envelope is the LDOS for the spin-(-1) states. The dark red curve represents the transmission characteristics for the spin-1 particles, the dark blue curve is for the spin-0 particles, and the dark green curve stands for the spin-(-1) particles. (a) is for $h = 3$, (b) is for $h = 4$, and (c) corresponds to $h = 6$. The lead parameters for the non-magnetic leads are $\epsilon_L = \epsilon_R = 0$ and $t_{LD} = t_{RD} = t_L = t_R = 4$.

corresponding to the different components of any higher spin. The results for spin 3/2 and spin 2 are shown in the supplemental material [40]. The basic mechanism of designing spin filters by controlling the value and the orientation of the magnetic moments of magnetic atoms in the chain remains the same as we move on to the higher spin states. For the higher spin states the number of spin channels increases, and we have a whole lot of options as to which spin component we want to make transmitting through the system for a certain energy regime. We need to tune the magnitude of h accordingly to have a spin filtering effect as we climb up to the higher spin states.

IV. TWO-TERMINAL TRANSPORT AND SPIN FILTERING

We now discuss the results of two-terminal transport across the magnetic chain. The detailed formulation of the method is provided in the Appendix. For simplicity, we plot the transmission coefficient in each case in the same figure as the corresponding LDOS. We start with the simple case of spin 1/2 and $\theta = 0$, and choose values of h such that there are (a) overlapping, (b) touching and (c) well-separated subbands. From Fig. 2(a) we see that the DOS of the 'up' and the 'down' spin states for $h = 1$ overlap over one third of the range of allowed eigenvalues. The corresponding transmission spectrum naturally offers a mixed character. There is a partial filtering effect with only 'up' spin electrons emerging out of the system in the energy interval $-3 \leq E \leq -1$, while it is the opposite in its positive counterpart. With $h = h_c = 2$, the subbands for the 'up' and 'down' spin states just touch each other. It is obvious from Fig. 2(b) that only 'up' spin electrons get transported in the lower half of the band, i.e., in the range $-4 \leq E \leq 0$, while the 'down' spin electrons transmit in the range $0 \leq E \leq 4$. With $h = 3$, the gap is explicit, and the spin filtering effect is clear. In this simple case, there is no 'spin flip' effect, and the 'up' ('down') electrons get transmitted precisely in the energy intervals in which the respective bands are populated. For $\theta = \pi/4$ the situation is more complicated as shown in Fig. 3. Here we see that for the same values of h as in Fig. 2, we now always get transport with mixed spin-up and spin-down components, even when there is a well-pronounced gap at shown in Fig. 3(c). Adjusting the value of θ therefore allows to control the relative admixture of the transported spin states while the choice of h determines the energy range in which the different transport channels will be open.

The behaviour shown for spin-1/2 persists for spin-1 (and higher spin states [40]) as shown Fig. 4 (a), (b) and (c) for $\theta = 0$. The gap opens at a larger value of h, as compared to the spin-1/2 case and can be easily estimated from Eq. (12). The DOS corresponding to the three spin components, namely, 1, 0 and -1, exhibit overlap in the panel (a) for $h = 3$. The critical value of $h = 4$ makes the subbands touch each other at the appropriate energy values, while a clean gap opens up as $h = 6$. Consequently, the two terminal transport exhibits a partial filtering in selected energy regimes in panel (a) while there is perfect filtering in (b) and (c). We note in (a) that the partial filtering in transmission exists only between the spin channels $(1, 0)$ and $(0, -1)$. The results can be understood intuitively if one recalls that $S = 1$ is identical to the case of a three strand ladder. Since we are working with nearest neighbor hopping in both the longitudinal and the transverse directions and rigid boundary conditions in the y-direction, the upper arm of the ladder (equivalent to the spin-1 channel) is totally decoupled from the lower arm (the spin-(-1) channel). The central arm, namely, the spin-0 channel is coupled to these two outer arms. The partial filtering is thus caused by contributions coming from the *interacting pair* of 'arms', or equivalently, the spin channels. Clearly, this argument extends also to the higher spin states.

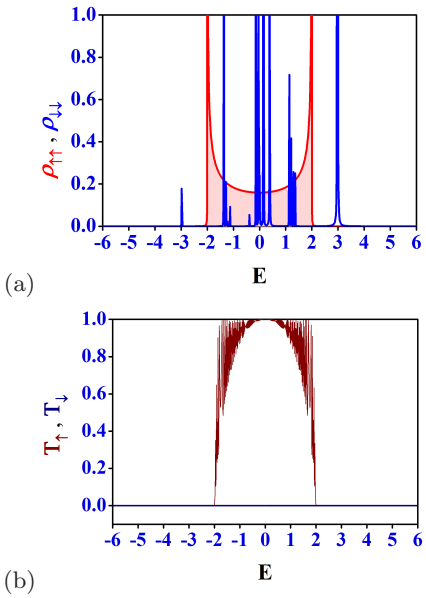

FIG. 5: (Color online) (a) Densities of states of the decoupled set of equations (13) when $\epsilon_n = h_n = \mu\cos(\pi Q n a)$ with $\mu = 1$ and $Q = (\sqrt{5}+1)/2$. The red and the blue lines correspond to the Eq. (13a) and Eq. (13b) respectively. (b) The zero transmission for the 'down' spins reflect the 'critical' character of the wavefunctions obtained from Eq. (13b), and the high transmission of the 'up' spins reveal the extended nature of the wavefunctions obtained from Eq. (13a), and represents a perfect spin filter. We have set $t = 1$, and energy is measured in units of t. The lattice constant $a = 1$.

V. SPIN FILTERING WITH CORRELATED DISORDER

A perfect spin filter can be designed even without setting constant values for the on-site potentials and the substrate magnetic moments, and without bothering about engineering gaps in the energy spectrum. This can be achieved by introducing correlations between the numerical values of $\epsilon_{n,\uparrow} = \epsilon_{n,\downarrow} = \epsilon_n$ and the magnitude of the substrate moments h_n. We demonstrate a special situation in Fig. 5. For simplicity, but without sacrificing the central spirit, we assign an Aubry-Andre variation [41] in the on-site potential, viz., $\epsilon_n = \mu\cos(\pi Q n a)$ with $Q = (\sqrt{5}+1)/2$. This distribution of the on-site potential leads to extended, critical or localized eigenstates for $\mu < 2t$, $\mu = 2t$ and $\mu > 2t$ respectively [41]. The distribution of the magnetic moments h_n are chosen to be equal to ϵ_n. In addition, we set $\theta_n = 0$. With the choice of $\theta_n = 0$, and $\epsilon_{n,\uparrow} = \epsilon_{n,\downarrow} = \epsilon_n$, the set of equations (3a) and (3b) map into the following set of equations,

$$(E - \epsilon_n + h_n)\,\psi_{n,\uparrow} = t\psi_{n+1,\uparrow} + t\psi_{n-1,\uparrow}, \qquad (13a)$$
$$(E - \epsilon_n - h_n)\,\psi_{n,\downarrow} = t\psi_{n+1,\downarrow} + t\psi_{n-1,\downarrow}. \qquad (13b)$$

With $\epsilon_n = h_n$, the 'effective' on-site potential in Eq. (13b) is equal to $2\mu\cos(\pi Q n a)$, and a selection of $\mu = 1$ makes the eigenstates corresponding to Eq. (13b) *critical*. Eq. (13a), with $\epsilon_n = h_n$, now represents a perfectly ordered chain with its spectrum ranging from $E = -2t$ to $E = 2t$. The densities of states and corresponding transport are shown in Fig. 5. In panel (a), the densities of states for the two decoupled channels are shown. The DOS for the original system is obtained by convolution of these two, but will definitely encompass the same energy regimes. The 'up' spins now have an absolutely continuous DOS shown by the red shaded curve, ranging between $[-2t, 2t]$. The critical eigenstates for the 'down' spins are shown by the blue lines. As critical and extended states can not coexist at the same energy, the central part of the spectrum will remain extended in the final, convolved DOS. The outer peaks however, will be there.

The corresponding transport characteristics are represented in panel (b). The total 'down' spin transport is naturally blocked, and we now have a clear case of spin filtering even with correlated, but a *deterministic disorder*, as is evident from the high transmission of 'up' spin states between $[-2t, 2t]$. It can be easily understood that, with a different choice of correlation between ϵ_n and h_n (say, $\epsilon_n = -h_n$), we can easily make the 'down' spin channel to be perfectly conducting, and the 'up' spins to be completely blocked. As we go to the higher spin cases, the same trick can be used to make one of the spin channels to be perfectly conducting and the rest to be completely blocked. Obviously we need to have different correlations between ϵ_n and h_n for different cases as we move along the higher spin ladder.

It is obvious that we need not stick to the case of deterministic disorder only. If we choose both ϵ_n and h_n in a random yet in correlated way, such that $\epsilon_n - h_n = \Lambda$ remains a constant, i.e., n-independent, then Eq. (9a) yields an absolutely continuous spectrum in the range $\Lambda - 2t \le E \le \Lambda + 2t$. This will be true even when the constant value of the polar angle $\theta \neq 0$. All eigenstates in this energy range have to be of extended Bloch functions. On the other hand, even with this choice, Eq. (9b) represents a randomly disordered chain of scatterers for which the *pseudoparticle states* with mixed spin status will be Anderson localized. The system will then open up a transmitting channel for such *mixed spin states* only in the window $\Lambda - 2t \le E \le \Lambda + 2t$, while it will remain opaque to all incoming electrons, irrespective of their spin states, in the energy regime beyond these limits [46].

The above argument holds, and the scenario may even become richer, as probes with higher spin states are incident on the magnetic substrate. For a total spin S, with the same restriction on the polar angle θ_n, and the azimuthal angle ϕ_n being set equal to zero, the matrix equation Eq. (4) decouples into a set of $2S+1$ independent equations, each representing a pseudoparticle with a mixed spin state (now much more complicated). One can then introduce a correlation between ϵ_n and h_n, keeping them individually random, so as to make any one of these independent equations (say, the central one) represent a perfectly ordered linear chain with its band ranging be-

tween two energy values dictated by the effective on-site potential in that equation. The remaining $2S$ equations represent disordered linear chains with all pseudoparticle states exponentially localized. The spectra arising out of these $2S$ linear chains have their own 'band centers' and can come arbitrarily close to the central continuum. The full spectrum is expected to be a dense packing of point-like distributions on either side of the central continuum. Considering the overall charge transport, such cases may even give rise to the possibility of a metal-insulator transition. The situation is to be contrasted with the case of a real multiple stranded ladder network [37] remembering that, here we have just a single magnetic chain. It is the spin state of the incoming particle that will decide whether such a simple quantum device will show up any reentrant behavior in charge transport or not.

VI. A SPIN SPIRAL: SIMULATING 'LOCAL' DISORDER

In this section we extend the concepts developed in the earlier sections to a patterned magnetic chain mimicking a spin spiral [42] in one dimension. The n-th atomic site

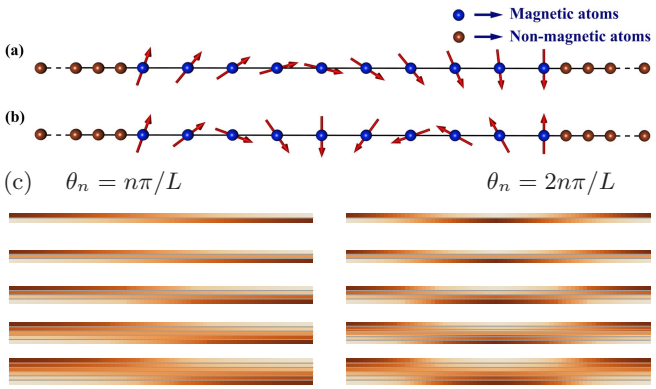

FIG. 6: (Color online) Schematic diagram of linear array of magnetic atoms (blue spheres) with magnetic moment vectors $\vec{h}$ (red arrows) forming spiral configurations for (a) $\theta_n = n\pi/L$ and (b) $2n\pi/L$. The system is connected between two non-magnetic semi-infinite leads (brown spheres). The horizontal lines are guides to the eye only. (c) Color representation of the on-site potential $h\cos\theta_n$ of spiral configurations at $L = 72$ for (left) $\theta_n = n\pi/L$ and (right) $2n\pi/L$ corresponding to $S = 1/2,\ 1,\ \ldots,\ 5/2$ from top to bottom. Dark colors correspond to large values.

now has its magnetic moment tilted with respect to the global magnetization axis (the z-axis) by an angle θ_n. As we neglect any spin-orbit interaction in this work, the spin and the position spaces are decoupled, and the relative orientation of the neighboring spin becomes important in respect of the transport and other physical properties. Here we stick to a periodic variation of the spiral, though the period can be quite arbitrary. The configuration is schematically depicted in Fig. 6 and can be identified as a *frozen* magnon. If we keep our attention confined to the 'chemical unit cell' only, the spiral configuration breaks the translational order locally (though preserving it globally of course) and simulates the effect of a kind of (deterministic) disorder, in particular, when the length of the chain is shorter than the period of the spin spiral. A study of the transmission characteristics for a spiral patch with length restricted to less than a period or its integral multiple, may show up some character expected for a real disordered magnetic chain, and test the robustness of the results obtained earlier.

We follow the same RSRG decimation scheme used earlier to study the LDOS at a bulk site for $\theta_n = n\pi/L$ and $\theta_n = n\pi/(L/2)$. Even when the strength of the magnetic moment h is set to be same at every magnetic site, the variation in θ_n naturally leads to variations in the values of $h\cos\theta_n$ and $h\sin\theta_n$. This implies that we have a magnetic chain of atoms with a (deterministic) fluctuation both in the effective on site potential, viz., $\epsilon \pm h\cos\theta_n$ and the 'coupling' $h\sin\theta_n$ between the 'up' and the 'down' spin channels. Mapping into the effective multi-strand ladder network, we have a case of a ladder where the 'rungs' are associated with varying hopping integrals, simulating a kind of deformation, and where, at the same time the vertices are occupied by atomic sites with sequentially changing on-site potentials, see Fig. 6(c).

In Fig. 7 we show the variation of the LDOS and corresponding transmission spectrum for a spin-1/2 spiral configuration. The periods of the spiral configurations are chosen to be 600 and 300 corresponding to Fig. 7(a), (b) and (c), (d) respectively. We have set $h = 2$ throughout and have taken $L = 300$. The energy bands for the 'up' and the 'down' spin channels touch each other at this h as in Figs. 2 and 3. However, in contradistinction to these previous results, we now observe a *spin-flipped transmission* in Fig. 7(a), and (b). This can be understood if we recall that the 'effective' on-site potentials for the 'up' and the 'down' spin electrons turn out to be $-h\cos(n\pi/L)$ and $h\cos(n\pi/L)$ respectively. The period of variation in θ_n is $2L$. Thus, for a system size equal to half the period, the incoming 'up' particle traverses the potential landscape *uphill*, as shown in Fig. 6(c). The transport of 'up' spin electrons thus experiences resistance in traversing the system, and is eventually blocked over the energy range $-4 < E < 0$, though $\rho_{\uparrow\uparrow}$ is finite here. On the other hand, the 'down' spin electrons effectively move *downhill* on the potential landscape, and are transmitted in the same energy range. The complementary picture is visible in Fig. 7(b). The specific choice of the polar angle $\theta_n = n\pi/L$ thus makes the L-atom long system a *spin flipper*.

The argument laid down here helps us understand the remaining two figures viz., Fig. 7 (c) and (d). We have now selected $\theta_n = n\pi/(L/2)$ and a system of length L offers a full period. The substrate atom at the first site $n = 0$ has its moment 'up'. As the probe reaches the end, the substrate moment is back in the 'up' orientation, fa-

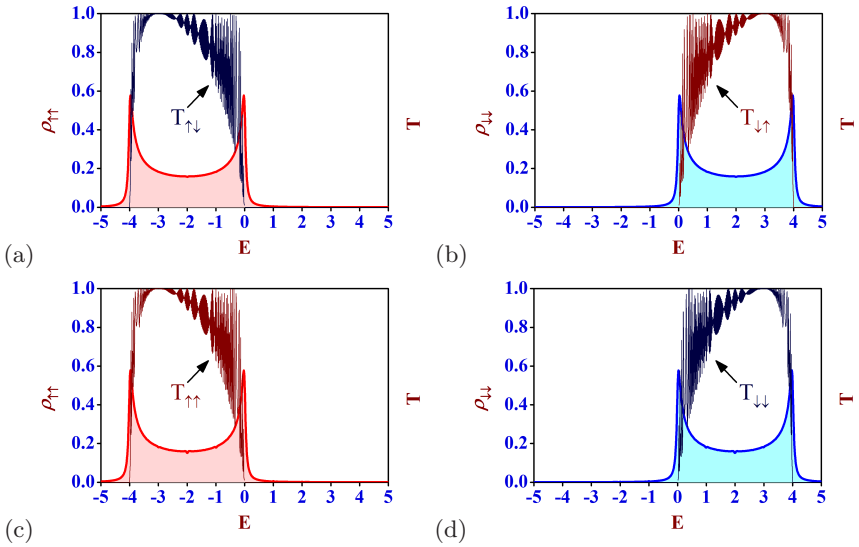

FIG. 7: (Color online) Plot of LDOS and transmission probabilities for spin-1/2 particles for spiral configurations of the magnetic moments in the magnetic chain system. The figures in the top panel [(a) and (b)] is for a variation of the angle $\theta_n = n\pi/L$, and the figures in the bottom panel [(c) and (d)] correspond to an angle variation $\theta_n = n\pi/(L/2)$ with $L = 300$. We have set $h = 2$ for all the magnetic sites in the chain.

voring the 'up' spin transport. The case is similar for the 'down' spin states, but in the complementary range of the energy. We do not have a spin flipper anymore. The results for higher spin S are presented in the supplement [40]. There will be m_S 'spin channels', e.g., for $S = 1$, the central channel, corresponding to the spin projection $m_S = 0$, turns out to be always transmitting, while the channels corresponding to $m_S = \pm 1$ exhibit spin-flipped transport for $\theta_n = n\pi/L$. The spin flipping character is lost if the system size includes a full period of variation in the polar angle θ_n, just as it was for the spin-1/2 case. We have also checked that a variation of the simple harmonic spiral variation presented here, using e.g. $\theta_n \propto \sqrt{n}$ or n^2, does not alter the overall spin-flipping presented here.

VII. CONCLUSION

In conclusion, we have presented a simple one dimensional chain of magnetic atoms which can act as spin filter or spin flipper for particles with arbitrary spins. The central idea depends crucially on a mapping of the problem for a spin-S particle into that of a $2S+1$ strand ladder network. The magnetic moment of the substrate atoms turns out to be equivalent to the 'inter-strand' tunnel hopping integral, which needs to be tailored to open up gaps in the DOS. This is shown to lead to the desired spin filtering effect. The analysis has been carried out for a wide variety of spins, going well beyond the standard spin-1/2 case. Higher spins are obtainable in appropriate atomic gases. The present work presents a unified model which can, in principle, through an appropriate substrate engineering, filter out arbitrarily large spin components, treating fermions and bosons on the same footing.

Talking about the experimental aspects of the work, the model system proposed by us can actually be realised now a days experimentally as well. With the present day advanced technologies people can image and manipulate the spin direction of individual magnetic atoms [43] to grow nanomagnets where exchange-coupled atomic magnetic moments form an array. Such tailor-made nanomagnets posses a rich variety of magnetic properties and can be explored as constituents of nanospintronics technologies [44]. So the model magnetic chains proposed by us are not far from reality. The concept of spin transport for higher spin states can be realised in atomic gases, and may lead to some exciting new generation spin-based devices. The idea of filtering out one of the spin components for a certain energy regime can have useful application in spin-based logic gates [45].

Acknowledgments

BP would like to thank DST, India and British Council for providing the financial support through a Newton-Bhabha Fellowship, and acknowledges the University of Warwick for their kind hospitality during his stay at Warwick. Special thanks must be given to all the members of DisQS group and Paramita Dutta for stimulating discussions during the course of this work. No new data sets were presented in this work as classified according to the UK open data policy.

Appendix: Formulations to obtain the transport characteristics

1. Spin 1/2 case

We have used the transfer matrix method (TMM) to get the transmission probabilities for different spin channels. In this appendix we present a detailed formulation of that. We can easily recast Eqs. (3a) and (3b) to have following matrix equation,

$$\begin{pmatrix} \psi_{n+1,\uparrow} \\ \psi_{n+1,\downarrow} \\ \psi_{n,\uparrow} \\ \psi_{n,\downarrow} \end{pmatrix} = \underbrace{\begin{pmatrix} \frac{(E-\epsilon_{n,\uparrow}+h_n\cos\theta_n)}{t} & \frac{h_n\sin\theta_n e^{-i\phi_n}}{t} & -1 & 0 \\ \frac{h_n\sin\theta_n e^{i\phi_n}}{t} & \frac{(E-\epsilon_{n,\downarrow}-h_n\cos\theta_n)}{t} & 0 & -1 \\ 1 & 0 & 0 & 0 \\ 0 & 1 & 0 & 0 \end{pmatrix}}_{\boldsymbol{P_n}} \begin{pmatrix} \psi_{n,\uparrow} \\ \psi_{n,\downarrow} \\ \psi_{n-1,\uparrow} \\ \psi_{n-1,\downarrow} \end{pmatrix}. \tag{A.1}$$

where $\boldsymbol{P_n}$ is the *transfer matrix* for the n-th site.

We have a system (magnetic chain) with N number of magnetic sites connected between two semi-infinite non-magnetic leads. So the matrix equation connecting the wave functions of the lead-system-lead bridge is given by,

$$\begin{pmatrix} \psi_{N+2,\uparrow} \\ \psi_{N+2,\downarrow} \\ \psi_{N+1,\uparrow} \\ \psi_{N+1,\downarrow} \end{pmatrix} = \underbrace{\boldsymbol{M_R}\cdot\boldsymbol{P}\cdot\boldsymbol{M_L}}_{\boldsymbol{M}} \begin{pmatrix} \psi_{0,\uparrow} \\ \psi_{0,\downarrow} \\ \psi_{-1,\uparrow} \\ \psi_{-1,\downarrow} \end{pmatrix}. \tag{A.2}$$

where $\boldsymbol{M_L}$ is the transfer matrix for the left lead, $\boldsymbol{M_R}$ is the transfer matrix for the right lead, $\boldsymbol{P} = \prod_{n=N}^{1} \boldsymbol{P_n}$, and $\boldsymbol{M}$ is the total transfer matrix for the lead-system-lead bridge.

2. *Evaluation of* $\boldsymbol{M_L}$

We have set $\epsilon_L = \epsilon_0$ for the all the sites in the left lead. The difference equation connecting the wave function amplitude of the 0-th site with that of the 1-th and -1-th sites is,

$$(E-\epsilon_0)\psi_0 = t_{LD}\psi_1 + t_L\psi_{-1}. \tag{A.3}$$

In the lead, according to the tight-binding model, we have $\psi_n = Ae^{ikna}$ and $\psi_0 = e^{i\gamma_L}\psi_{-1}$, where $\gamma_L = ka$ and $E = \epsilon_0 + 2t_L\cos\gamma_L$. Consequently we find $\psi_1 = \left(t_L e^{i\gamma_L}/t_{LD}\right)\psi_0$. In TMM form, this gives

$$\begin{pmatrix} \psi_{1,\uparrow} \\ \psi_{1,\downarrow} \\ \psi_{0,\uparrow} \\ \psi_{0,\downarrow} \end{pmatrix} = \underbrace{\begin{pmatrix} \frac{t_L}{t_{LD}}e^{i\gamma_L} & 0 & 0 & 0 \\ 0 & \frac{t_L}{t_{LD}}e^{i\gamma_L} & 0 & 0 \\ 0 & 0 & e^{i\gamma_L} & 0 \\ 0 & 0 & 0 & e^{i\gamma_L} \end{pmatrix}}_{\boldsymbol{M_L}} \begin{pmatrix} \psi_{0,\uparrow} \\ \psi_{0,\downarrow} \\ \psi_{-1,\uparrow} \\ \psi_{-1,\downarrow} \end{pmatrix}. \tag{A.4}$$

3. *Evaluation of* $\boldsymbol{M_R}$

We set $\epsilon_R = \epsilon_0$ for the all the sites in the right lead. The difference equation connecting the wave function amplitude of the $(N+1)$-th site with that of the $(N+2)$-th and N-th sites is,

$$(E-\epsilon_0)\psi_{N+1} = t_R\psi_{N+2} + t_{RD}\psi_N, \tag{A.5}$$

where $\psi_{N+2} = Ae^{ik(N+2)a}$; $\psi_{N+2} = e^{i\gamma_R}\psi_{N+1}$, and $\gamma_R = ka$ and $E = \epsilon_0 + 2t_R\cos\gamma_R$. Consequently, $\psi_{N+1} = \left(t_{RD}e^{i\gamma_R}/t_R\right)\psi_N$ and

$$\begin{pmatrix} \psi_{N+2,\uparrow} \\ \psi_{N+2,\downarrow} \\ \psi_{N+1,\uparrow} \\ \psi_{N+1,\downarrow} \end{pmatrix} = \underbrace{\begin{pmatrix} e^{i\gamma_R} & 0 & 0 & 0 \\ 0 & e^{i\gamma_R} & 0 & 0 \\ 0 & 0 & \frac{t_{RD}}{t_R}e^{i\gamma_R} & 0 \\ 0 & 0 & 0 & \frac{t_{RD}}{t_R}e^{i\gamma_R} \end{pmatrix}}_{\boldsymbol{M_R}} \begin{pmatrix} \psi_{N+1,\uparrow} \\ \psi_{N+1,\downarrow} \\ \psi_{N,\uparrow} \\ \psi_{N,\downarrow} \end{pmatrix}. \tag{A.6}$$

a. An incoming spin up (↑)

If the incoming particle to the left electrode (lead) has a spin-up (↑) projection then the wavefunction amplitudes in Eq. (A.2) can be written as, $\psi_{-1,\uparrow} = e^{-i\gamma_L} + \mathcal{R}_{\uparrow\uparrow}e^{i\gamma_L}$, $\psi_{-1,\downarrow} = \mathcal{R}_{\uparrow\downarrow}e^{i\gamma_L}$, $\psi_{0,\uparrow} = 1 + \mathcal{R}_{\uparrow\uparrow}$, $\psi_{0,\downarrow} = \mathcal{R}_{\uparrow\downarrow}$, $\psi_{N+2,\uparrow} = \mathcal{T}_{\uparrow\uparrow}e^{i(N+2)\gamma_R}$, $\psi_{N+2,\downarrow} = \mathcal{T}_{\uparrow\downarrow}e^{i(N+2)\gamma_R}$, $\psi_{N+1,\uparrow} = \mathcal{T}_{\uparrow\uparrow}e^{i(N+1)\gamma_R}$, $\psi_{N+1,\downarrow} = \mathcal{T}_{\uparrow\downarrow}e^{i(N+1)\gamma_R}$, where $\mathcal{R}_{\uparrow\uparrow(\uparrow\downarrow)}$ and $\mathcal{T}_{\uparrow\uparrow(\uparrow\downarrow)}$ are the amplitudes of the reflected and transmitted electron wavefunctions with spin-up (↑) projection, which remain in spin-up (↑) state (or, flip to spin-down (↓) state) after passing through the system. If we put the above values of the wavefunction amplitudes in Eq. (A.2) then we will have

$$\begin{pmatrix} \mathcal{T}_{\uparrow\uparrow}e^{i(N+2)\gamma_R} \\ \mathcal{T}_{\uparrow\downarrow}e^{i(N+2)\gamma_R} \\ \mathcal{T}_{\uparrow\uparrow}e^{i(N+1)\gamma_R} \\ \mathcal{T}_{\uparrow\downarrow}e^{i(N+1)\gamma_R} \end{pmatrix} = \boldsymbol{M} \begin{pmatrix} 1+\mathcal{R}_{\uparrow\uparrow} \\ \mathcal{R}_{\uparrow\downarrow} \\ e^{-i\gamma_L}+\mathcal{R}_{\uparrow\uparrow}e^{i\gamma_L} \\ \mathcal{R}_{\uparrow\downarrow}e^{i\gamma_L} \end{pmatrix}. \quad \text{(A.7)}$$

We solve Eq. (A.7) for $\mathcal{T}_{\uparrow\uparrow}$ and $\mathcal{T}_{\uparrow\downarrow}$ and obtain the transmission probabilities as

$$T_{\uparrow\uparrow} = \frac{t_R \sin\gamma_R}{t_L \sin\gamma_L}\left|\mathcal{T}_{\uparrow\uparrow}\right|^2, \quad T_{\uparrow\downarrow} = \frac{t_R \sin\gamma_R}{t_L \sin\gamma_L}\left|\mathcal{T}_{\uparrow\downarrow}\right|^2. \quad \text{(A.8)}$$

The total transmission probability for a spin-up (↑) particle is given by,

$$T_{\uparrow} = T_{\uparrow\uparrow} + T_{\uparrow\downarrow}. \quad \text{(A.9)}$$

b. An incoming spin down (↓)

If the incoming particle to the left electrode (lead) has a spin down (↓) projection then $\psi_{-1,\uparrow} = \mathcal{R}_{\downarrow\uparrow}e^{i\gamma_L}$, $\psi_{-1,\downarrow} = e^{-i\gamma_L} + \mathcal{R}_{\downarrow\downarrow}e^{i\gamma_L}$, $\psi_{0,\uparrow} = \mathcal{R}_{\downarrow\uparrow}$, $\psi_{0,\downarrow} = 1 + \mathcal{R}_{\downarrow\downarrow}$, $\psi_{N+2,\uparrow} = \mathcal{T}_{\downarrow\uparrow}e^{i(N+2)\gamma_R}$, $\psi_{N+2,\downarrow} = \mathcal{T}_{\downarrow\downarrow}e^{i(N+2)\gamma_R}$, $\psi_{N+1,\uparrow} = \mathcal{T}_{\downarrow\uparrow}e^{i(N+1)\gamma_R}$, $\psi_{N+1,\downarrow} = \mathcal{T}_{\downarrow\downarrow}e^{i(N+1)\gamma_R}$, where $\mathcal{R}_{\downarrow\downarrow(\downarrow\uparrow)}$ and $\mathcal{T}_{\downarrow\downarrow(\downarrow\uparrow)}$ are the amplitudes of the reflected and transmitted electron wavefunctions with spin-down (↓) projection, which remain in spin-down (↓) state (or, flip to spin-up (↑) state) after passing through the system. As before, we find

$$\begin{pmatrix} \mathcal{T}_{\downarrow\uparrow}e^{i(N+2)\gamma_R} \\ \mathcal{T}_{\downarrow\downarrow}e^{i(N+2)\gamma_R} \\ \mathcal{T}_{\downarrow\uparrow}e^{i(N+1)\gamma_R} \\ \mathcal{T}_{\downarrow\downarrow}e^{i(N+1)\gamma_R} \end{pmatrix} = \boldsymbol{M} \begin{pmatrix} \mathcal{R}_{\downarrow\uparrow} \\ 1+\mathcal{R}_{\downarrow\downarrow} \\ \mathcal{R}_{\downarrow\uparrow}e^{i\gamma_L} \\ e^{-i\gamma_L}+\mathcal{R}_{\downarrow\downarrow}e^{i\gamma_L} \end{pmatrix}. \quad \text{(A.10)}$$

and solve Eq. (A.10) for $\mathcal{T}_{\downarrow\downarrow}$ and $\mathcal{T}_{\downarrow\uparrow}$. The transmission probabilities are now

$$T_{\downarrow\downarrow} = \frac{t_R \sin\gamma_R}{t_L \sin\gamma_L}\left|\mathcal{T}_{\downarrow\downarrow}\right|^2, \quad T_{\downarrow\uparrow} = \frac{t_R \sin\gamma_R}{t_L \sin\gamma_L}\left|\mathcal{T}_{\downarrow\uparrow}\right|^2, \quad \text{(A.11)}$$

with total transmission probability for a spin-down (↓) particle

$$T_{\downarrow} = T_{\downarrow\downarrow} + T_{\downarrow\uparrow}. \quad \text{(A.12)}$$

4. An example for higher spin cases: spin 1

Proceeding in the same way as in the spin-1/2 case, we obtain the following forms of the transfer matrices for the left and right leads as, $\boldsymbol{M_L} = e^{i\gamma_L}\mathrm{diag}\,(t_L/t_{LD}, t_L/t_{LD}, t_L/t_{LD}, 1, 1, 1)$ and $\boldsymbol{M_R} = e^{i\gamma_R}\mathrm{diag}\,(1, 1, 1, t_R/t_{RD}, t_R/t_{RD}, t_R/t_{RD})$. The transfer matrix for spin-1 particles at the n-th site reads as,

$$\boldsymbol{P_n} = \begin{pmatrix} \frac{(E-\epsilon_{n,1}+h_n\cos\theta_n)}{t} & \frac{h_n\sin\theta_n e^{-i\phi_n}}{\sqrt{2}t} & 0 & -1 & 0 & 0 \\ \frac{h_n\sin\theta_n e^{i\phi_n}}{\sqrt{2}t} & \frac{(E-\epsilon_{n,0})}{t} & \frac{h_n\sin\theta_n e^{-i\phi_n}}{\sqrt{2}t} & 0 & -1 & 0 \\ 0 & \frac{h_n\sin\theta_n e^{i\phi_n}}{\sqrt{2}t} & \frac{(E-\epsilon_{n,-1}-h_n\cos\theta_n)}{t} & 0 & 0 & -1 \\ 1 & 0 & 0 & 0 & 0 & 0 \\ 0 & 1 & 0 & 0 & 0 & 0 \\ 0 & 0 & 1 & 0 & 0 & 0 \end{pmatrix}. \quad \text{(A.13)}$$

Similar to the spin-1/2 particles, we obtain the transmission probabilities for the spin-1 particles as,

$$T_{\sigma\sigma'} = \frac{t_R \sin\gamma_R}{t_L \sin\gamma_L}\left|\mathcal{T}_{\sigma\sigma'}\right|^2, \quad \text{(A.14)}$$

where $\sigma, \sigma' = 1, 0, -1$, and the total transmission probabilities for spin 1, 0, and -1 components respectively are

given by,

$$T_1 = T_{1,1} + T_{1,0} + T_{1,-1}, \tag{A.15a}$$
$$T_0 = T_{0,1} + T_{0,0} + T_{0,-1}, \tag{A.15b}$$
$$T_{-1} = T_{-1,1} + T_{-1,0} + T_{-1,-1}. \tag{A.15c}$$

Clearly, this scheme can be carried forward to obtain the transport characteristics for particles with any arbitrary spin. For spin $S = 1/2$ in (A.1) and for $S = 1$ in (A.13), the on-site magnetic strength coefficients $\propto \cos\theta_n$ are 1, -1 and 1, 0, -1, respectively. For $S = 3/2$, we have $1, 1/3, -1/3, -1$, for $S = 2$ they are $1, 1/2, 0, -1/2, -1$ and for $S = 5/2$, we have $1, 3/5, 1/5, -1/5, -3/5, -1$. The proportionality coefficients for the hopping $\propto \sin\theta_n$ are 1 for $S = 1/2$, and $1/\sqrt{2}, 1/\sqrt{2}$ for $S = 1$ in (A.1) and (A.13), respectively. For $S = 3/2$, we find $1/\sqrt{3}, 2/3, 1/\sqrt{3}$, for $S = 2$ they are $1/2, \sqrt{6}/4, \sqrt{6}/4, 1/2$ and, last, for $S = 5/2$ we have $1/\sqrt{5}, \sqrt{8}/5, 3/5, \sqrt{8}/5, 1/\sqrt{5}$. These coefficients, for the $\cos\theta_n$ terms, are used in Fig. 6(c).

[1] G. A. Prinz, Phys. Today **48**, 58 (1995); Science **282**, 1660 (1998).
[2] S. A. Wolf, D. D. Awschalom, R. A. Buhrman, J. M. Daughton, S. von Molnár, M. L. Roukes, A. Y. Chtchekanova, and D. M. Treger, Science **294**, 1488 (2001).
[3] M. Julliere, Phys. Lett. A **54**, 225 (1975).
[4] J. S. Moodera, L. R. Kinder, T. M. Wong, and R. Meservey, Phys. Rev. Lett. **74**, 3273 (1995).
[5] M. N. Baibich, J. M. Broto, A. Fert, F. N. Van Dau, F. Petroff, P. Etienne, G. Creuzet, A. Friederich, and J. Chazelas, Phys. Rev. Lett. **61**, 2472 (1988).
[6] D. Goldhaber-Gordon, H. Shtrikman, D. Mahalu, D. Abusch-Magder, U. Meirav, and M. A. Kastner, Nature (London) **391**, 156 (1998).
[7] S. M. Cronenwett, T. H. Oosterkamp, and L. P. Kouwenhoven, Science **281**, 540 (1998).
[8] H. Yu and J.-Q. Liang, Phys. Rev. B **72**, 075351 (2005).
[9] L. P. Rokhinson, V. Larkina, Y. B. Lyanda-Geller, L. N. Pfeiffer, and K. W. West, Phys. Rev. Lett. **93**, 146601 (2004).
[10] N. Tombros, C. Jozsa, M. Popinciuc, H. T. Jonkman, and B. J. Van Wees, Nature **448**, 571 (2007).
[11] S. K. Watson, R. M. Potok, C. M. Markus, and V. Umansky, Phys. Rev. Lett. **91**, 258301 (2003).
[12] E. R. Mucciolo, C. Chamon, and C. M. Marcus, Phys. Rev. Lett. **89**, 146802 (2002).
[13] V. Rodrigues, J. Bettini, P. C. Silva, and D. Ugarte, Phys. Rev. Lett. **91**, 096801 (2003).
[14] J. E. Birkholz and V. Meden, Phys. Rev. B **79**, 085420 (2009).
[15] R. P. Andres, T. Bein, M. Dorogi, S. Feng, J. I. Henderson, C. P. Kubiak, W. Mahoney, R. G. Osifchin, and R. Reifenberger, Science **272**, 1323 (1996).
[16] N. Sergueev, Q.-feng Sun, H. Guo, B. G. Wang, and J. Wang, Phys. Rev. B **65**, 165303 (2002).
[17] H.-F. Lü, S.-S. Ke, X.-T. Zu, and H.-W. Zhang, J. Appl. Phys. **109**, 054305 (2011).
[18] R. Wang and J.-Q. Liang, Phys. Rev. B **74**, 144302 (2006).
[19] A. A. Shokri and M. Mardaani, Solid State Comm. **137**, 53 (2006).
[20] A. A. Shokri, M. Mardaani, and K. Esfarjani, Physica E **27**, 325 (2005).
[21] M. Mardaani and A. A. Shokri, Chem. Phys. **324**, 541 (2006).
[22] M. Dey, S. K. Maiti, and S. N. Karmakar, Phys. Lett. A **374**, 1522 (2010).
[23] M. Dey, S. K. Maiti, and S. N. Karmakar, Eur. Phys. J. B **80**, 105 (2011).
[24] M. Dey, S. K. Maiti, and S. N. Karmakar, J. Comput. and Theo. Nanosc. **8**, 253 (2011).
[25] C. Núñez, F. Domínguez-Adame, P. A. Orellana, L. Rosales, and R. A. Römer, 2D Mater. **3**, 025006 (2016).
[26] C. Betthausen, T. Dollinger, H. Saarikoski, V. Kolkovsky, G. Karczewski, T. Wojtowicz, K. Richter, and D. Weiss, Science **337**, 324 (2012).
[27] H. Saarikoski, T. Dollinger, and K. Richter, Phys. Rev. B **86**, 165407 (2012).
[28] P. Wójcik, J. Adamowski, M. Wooszyn, and B. J. Spisak, Semicond. Sci. Technol. **30**, 065007 (2015).
[29] J. L. Pichard and G. Sarma, J. Phys. Colloques **42**, C4-37 (1981).
[30] A. MacKinnon and B. Kramer, Z. Phys. B **53**, 1 (1983).
[31] Y. Jiang, X. Guan, J. Cao, and H.-Q. Lin, Nucl. Phys. B **895**, 206 (2015).
[32] G. Pagano *et al.*, Nat. Phys. **10**, 198 (2014).
[33] M. Fattori, T. Koch, S. Goetz, A. Griesmaier, S. Hensler, J. Stuhler, and T. Pfau, Nat. Phys. **2**, 765 (2006).
[34] S. Sil, S. K. Maiti, and A. Chakrabarti, Phys. Rev. Lett. **101**, 076803 (2008).
[35] S. Sil, S. K. Maiti, and A. Chakrabarti, Phys. Rev. B **78**, 113103 (2008).
[36] B. Pal and A. Chakrabarti, Physica E **60**, 188 (2014).
[37] A. Rodriguez, A. Chakrabarti, and R. A. Römer, Phys. Rev. B **86**, 085119 (2012).
[38] A. Chakrabarti, S. N. Karmakar, and R. K. Moitra, Mod. Phys. Lett. B **4**, 795 (1990).
[39] M. Leadbeater, R. A. Römer, and M. Schreiber, Eur. Phys. J. B **8**, 643 (1999).
[40] See Supplemental Material at [URL will be inserted by publisher] for higher spin results.
[41] S. Aubry and G. André, Ann. Israel Phys. Soc. **3**, 133 (1980).
[42] J. Enkovaara, A. Ayuela, J. Jalkanen, L. Nordström, and R. M. Nieminen, Phys. Rev. B **67**, 054417 (2003).
[43] D. Serrate, P. Ferriani, Y. Yoshida, S.-W. Hla, M. Menzel, K. von Bergmann, S. Heinze, A. Kubetzka, and R. Wiesendanger, Nat. Nanotechnol. **5**, 350 (2010).
[44] A. A. Khajetoorians, J. Wiebe, B. Chilian, S. Lounis, S. Blügel, and R. Wiesendanger, Nat. Phys. **8**, 497 (2012).
[45] A. A. Khajetoorians, J. Wiebe, B. Chilian, and R. Wiesendanger, Science **332**, 1162 (2011).
[46] The same argument can of course be made when choos-

ing $\epsilon_n + h_n = \Lambda$. Then Eq. (9b) yields an absolutely continuous spectrum and Eq. (9a) represents a randomly disordered chain. Of course, the pertinent issue in this case is not filtering out a particular spin state. Instead, one can address a serious issue of localization to delocalization crossover for a pseudoparticle of a mixed spin state.

Spin filter for arbitrary spins by substrate engineering: supplemental material

Biplab Pal,[1,*] Rudolf A. Römer,[2,†] and Arunava Chakrabarti[1,‡]

[1] *Department of Physics, University of Kalyani, Kalyani, West Bengal-741235, India*
[2] *Department of Physics and Centre for Scientific Computing, University of Warwick, Coventry, CV4 7AL, UK*

In this supplemental material we present the figures for higher spin states – both for the constant values of the polar angle θ as well as for a 'spiral' configuration in θ. These results are complementary to the results discussed in the main paper. The methods and mathematical framework we have used to obtain these results are already discussed in the main paper.

I. CONSTANT POLAR ANGLE θ

In this section we present the results for constant polar angle θ. In Fig. S1 we show the local density of states (LDOS) and the corresponding two terminal transmission coefficient for a fixed $\theta = \pi/4$ and for different values of the strength of the magnetic moment h. This figure is the counter part of Fig. 4 in the main text for non-zero value of θ. In Fig. S2 and Fig. S3 we have exhibited a similar analysis corresponding to the spin-3/2 and spin-2 cases for $\theta = 0$. These two figures are complementary to the Figs. 2 and 4 given in the main article but now for higher spin states. Here we have a larger number of bands corresponding to different spin channels as the number of spin components has increased. The central idea remains the same as discussed in the main paper for spin-1/2 and spin-1 cases.

II. SPIRAL CASES

In Fig. S4, and Fig. S5 we show results for the LDOS and transmission characteristics corresponding to spins $S = 1$ and $S = 3/2$, respectively, for a *spiral* configuration of the local magnetic moments. These two figures are in connection to Fig. 7 in the main paper. Similar to the main paper, here also we get a spin flip transmission for a half period in the spiral configuration in the orientation of the local magnetic moments as compared to system length, and the phenomenon of spin flipping disappears for full period in spiral as compared to the system size. For the spin-1 case, the central spin channel corresponding to the spin-0 component does not exhibit this feature of spin flipping as h has no role to play for the spin-0 component. We have verified that the same thing happens for the spin-2 case as well but we have refrained from exhibiting those figures here since the main idea is easily understood from the results of the spin-1 case. For spin-3/2, the phenomena of spin flipping happens as well and a particle with a certain spin component flips to its counter part.

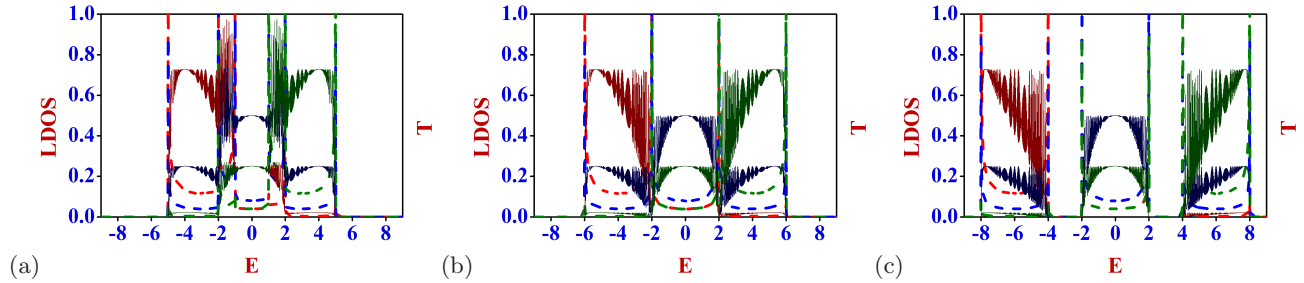

FIG. S1: (Color online) Variation of LDOS and transmission probabilities with energy E as a function of h for a fixed value of $\theta = \pi/4$ for spin-1 particles. The curves with the red dashed line represent the LDOS for the spin-1 states, the curves with the blue dashed line represent the LDOS for the spin-0 states, and the the curves with the green dashed line represent the LDOS for the spin-(-1) states. The dark red curve represents the transmission probability for the spin-1 particles, dark blue curve represents the transmission probability for the spin-0 particles,the dark green curve is exhibiting the transmission probability for the spin-(-1) particles. (a) is for $h = 3$, (b) is for $h = 4$, and (c) corresponds to $h = 6$. The lead parameters for the non-magnetic leads are $\epsilon_L = \epsilon_R = 0$ and $t_{LD} = t_{RD} = t_L = t_R = 4$.

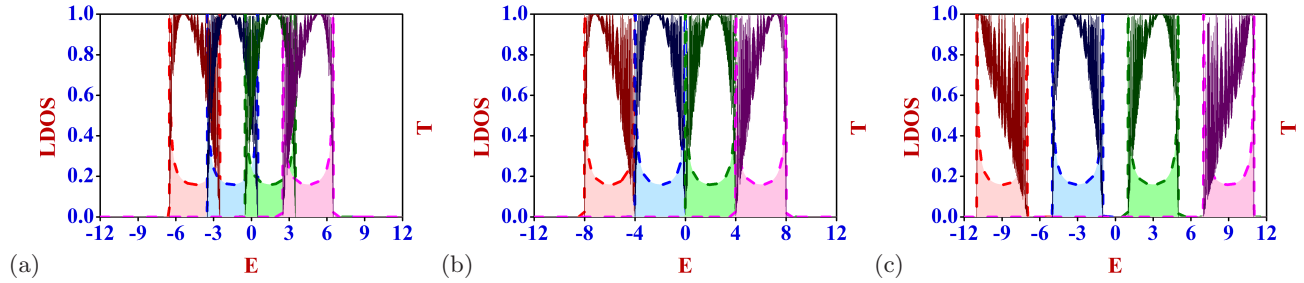

FIG. S2: (Color online) Variation of LDOS and transmission probabilities with energy E as a function of h for a fixed value of $\theta = 0$ for spin-3/2 particles. The light red shaded plot with the dashed red envelope is the LDOS for the spin-3/2 states, the light blue shaded plot with the blue dashed envelope is the LDOS for the spin-1/2 states, the light green shaded plot with the green dashed envelope is the LDOS for the spin-$(-1/2)$ states, and the light magenta shaded plot with the magenta dashed envelope is the LDOS for the spin-$(-3/2)$ states. The dark red curve represents the transmission characteristics for the spin-3/2 particles, the dark blue curve is for the spin-1/2 particles, the dark green curve is for the spin-$(-1/2)$ particles, and the dark magenta curve is for the spin-$(-3/2)$ particles. (a) is for $h = 4.5$, (b) is for $h = 6$, and (c) corresponds to $h = 9$. The lead parameters for the non-magnetic leads are $\epsilon_L = \epsilon_R = 0$ and $t_{LD} = t_{RD} = t_L = t_R = 6$.

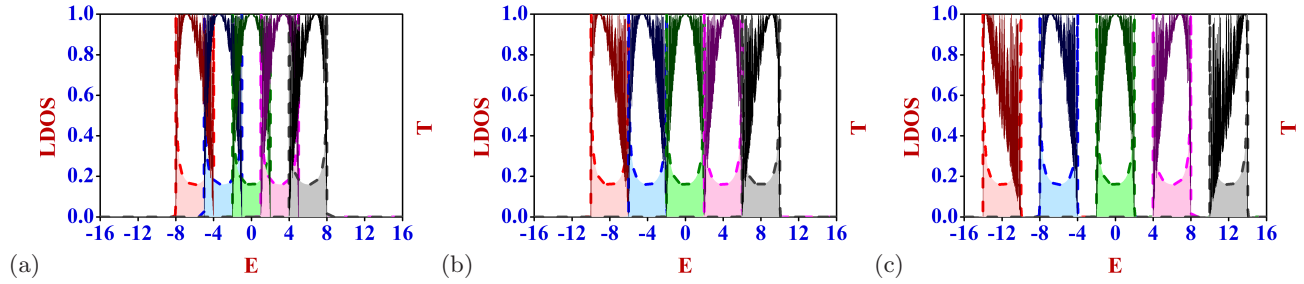

FIG. S3: (Color online) Variation of LDOS and transmission probabilities with energy E as a function of h for a fixed value of $\theta = 0$ for spin-2 particles. The light red shaded plot with the dashed red envelope is the LDOS for the spin-2 states, the light blue shaded plot with the blue dashed envelope is the LDOS for the spin-1 states, the light green shaded plot with the green dashed envelope is the LDOS for the spin-0 states, the light magenta shaded plot with the magenta dashed envelope is the LDOS for the spin-(-1) states, and the light gray shaded plot with the dark gray dashed envelope is the LDOS for the spin-(-2) states. The dark red curve represents the transmission characteristics for the spin-2 particles, the dark blue curve is for the spin-1 particles, the dark green curve is for the spin-0 particles, the dark magenta curve is for the spin-(-1) particles, and the black curve is for spin-(-2) particles. (a) is for $h = 6$, (b) is for $h = 8$, and (c) corresponds to $h = 12$. The lead parameters for the non-magnetic leads are $\epsilon_L = \epsilon_R = 0$ and $t_{LD} = t_{RD} = t_L = t_R = 8$.

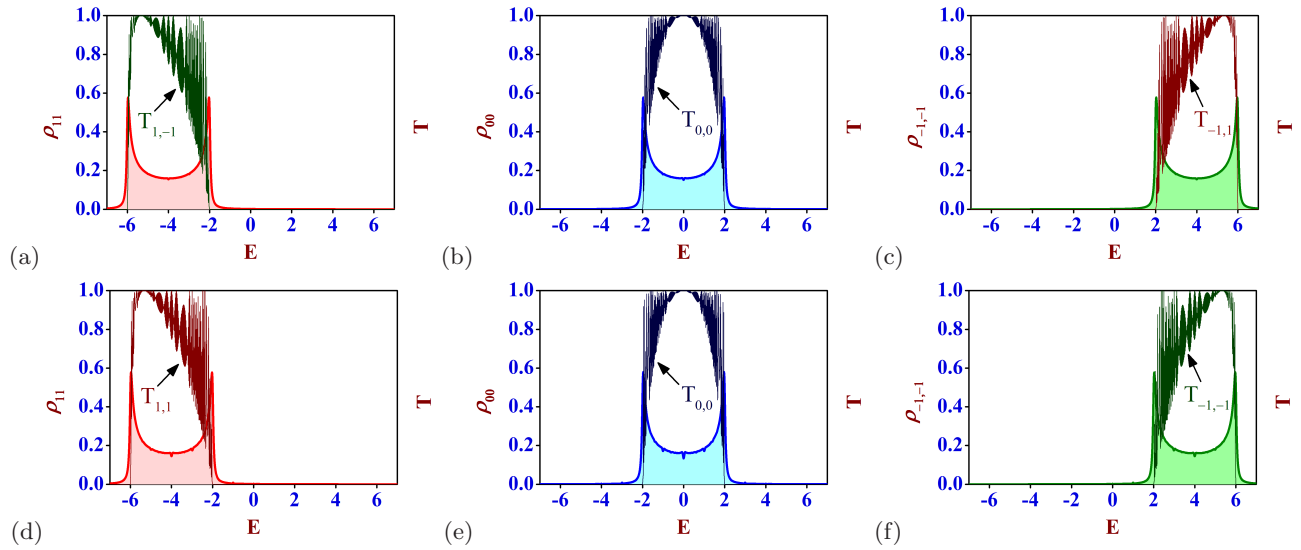

FIG. S4: (Color online) Plot of LDOS and transmission probabilities for spin-1 particles for spiral configurations of the magnetic moments in the magnetic chain system. The figures in the top panel [(a), (b) and (c)] is for a variation of the angle $\theta_n = n\pi/L$, and the figures in the bottom panel [(d), (e) and (f)] correspond to an angle variation $\theta_n = n\pi/(L/2)$ with $L = 300$. We have set $h = 4$ for all the magnetic sites in the chain.

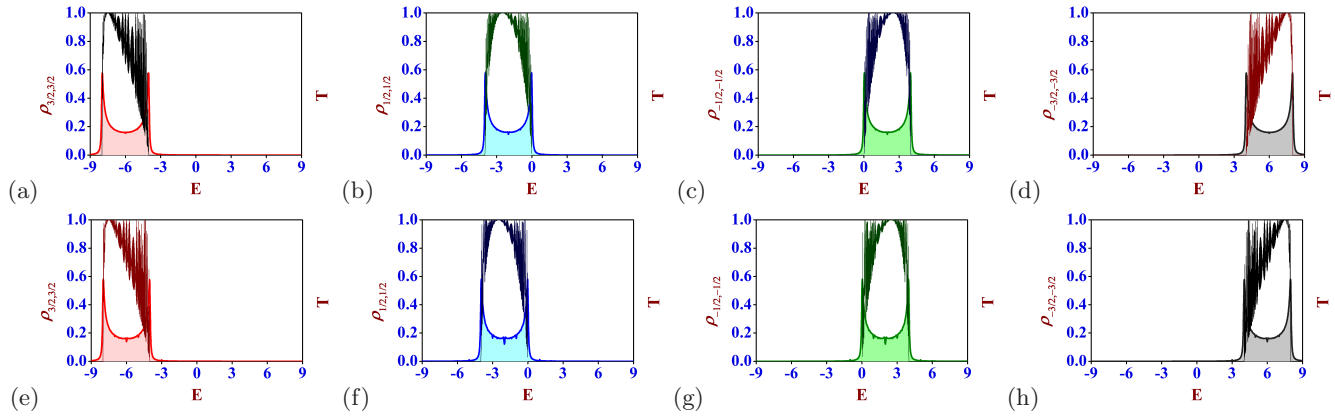

FIG. S5: (Color online) Plot of LDOS and transmission probabilities for spin-3/2 particles for spiral configurations of the magnetic moments in the magnetic chain system. The figures in the top panel [(a), (b), (c) and (d)] is for a variation of the angle $\theta_n = n\pi/L$, and the figures in the bottom panel [(e), (f), (g) and (h)] correspond to an angle variation $\theta_n = n\pi/(L/2)$ with $L = 300$. We have set $h = 6$ for all the magnetic sites in the chain.